Spinel-silicate melt partitioning of platinum group elements (PGEs) as a function of oxygen fugacity

Veronika Homolova
University of Toronto
2008

Supervisor: James Brenan

Abstract from GAC MAC

Experiments have been performed to measure PGE partitioning between spinel and silicate melt to better constrain the behaviour of these elements in sulfur-poor igneous systems. Partition coefficients (D-values) for all PGEs were determined from experiments performed in a gas mixing furnace over the fO_2 range from ~FMQ+ to FMQ+7, with samples suspended in a wire loop and CO_2-CO-N_2-air-O_2 mixtures used to control fO_2. Experiments to measure Os partitioning were performed at 1.3 GPa with samples encapsulated in Pt, and fO_2 fixed using Ru-RuO_2 (~FMQ+6) or Re-ReO_x (~FMQ+1) internal buffers. All experiments involved an initial superliquidus homogenization, then a time-temperature history designed to promote the growth of large crystals. The PGE content of run-product phases was determined by LA-ICPMS using synthetic glass and sulfide standards. Spinel D-values for Rh are found to be constant at ~140 over the fO_2 range of FMQ+3.5 to +7, despite changes in Rh oxidation state for this fO_2 interval predicted by metal solubility experiments. Spinel D-values for Pd are < 1 for the entire fO_2 range investigated, and become smaller with decreasing fO_2. This change in D-value for Pd can be modeled quantitatively using Pd^{1+} and Pd^{2+} speciation in the melt determined from solubility studies. Pt solubility studies infer that this element is likely to be predominantly 2+ in our experiments, and from ionic radius and charge considerations is therefore expected to behave compatibly in spinel. Measured D-values are <1, except at the highest fO_2s, likely reflecting the preference of Pt^{2+} for square planar, rather than octahedral coordination. We present the first Os partition coefficients of ~2 for spinel at FMQ+6.

Introduction

The platinum group elements display fractionated chondrite-normalized ratios in cumulate, crustal and some upper mantle rocks, unlike in most mantle derived rocks which show chondritic relative abundances [1]. This fractionation, which commonly parts the more refractory IPGE's (Os, Ir, Ru) from the less refractory PPGE's (Rh, Pt, Pd), is thought to be controlled by 1) the incongruent melting of base metals sulphides in the mantle, where IPGE bearing sulphides require higher degrees of melting than PPGE bearing sulphides 2) the

formation of PGMs which preferentially concentrate either IPGE's or PPGE's or 3) the larger D's of the IPGE's into early forming silicate and oxide phases, such as olivine and spinel [2]. Since sulphide/silicate melt D's of the PGE's are in the order of 10^4 and (silicate and oxide)/silicate melt D's are much lower, the influence of olivine and spinel crystallization in natural systems is more pronounced in sulphide-undersaturated systems [3]. The focus of this report is to better constrain the effect of spinel in fractionating the PGEs during sulphide-undersaturated petrogenesis.

The ability of spinel to fractionate the PGE's has been well documented in natural systems. In a recent study of highly depleted, BMS-free spinel harzburgites, Cr-spinel was found to contain the highest concentration of Ru and both olivine and Cr-spinel contained the highest concentrations of Os and Ir [4]. These latter concentrations, however, varied by an order of magnitude in spinel and were thought to be more readily explained by PGM inclusions [4]. In another study of mantle derived spinel and garnet lherzolites, spinel was found to be the most abundant in Pd and Ir and despite the poor correlation of Cr and Ir, the PGE's were believed to be in solid solution with spinel [5].

In a study of komatiitic basalts, Ir was shown to correlate with Cr, Mg# and Ni and it was suggested that to fully account for the calculated bulk D_{Ir} of 6, some Ir must have partitioned into either olivine or chromite [6]. In a different komatiite study, analysis of mineral separates demonstrated that chromites were more abundant in PGE's than olivines by two orders of magnitude and yielded partition coefficients for chromite of $D_{Ru,Os}$=150, D_{Ir}=100, D_{Pt}=3 and D_{Pd}=1.6 [7].

Chromites from podiform chromitiites of mantle peridotites have been examined and show high concentrations of IPGE's and depletions of PPGE's [8]. Interestingly, the high-Cr chromites are revealed to contain higher concentrations of Os, Ir, Ru, and Rh than the high-Al chromites yet, there was, however, no overall correlation between Cr and the PGE's and so, the authors state that it is uncertain whether the PGE's were in solid solution with chromite [8].

An overt problem in the aforementioned studies is the use of bulk analytical techniques to determine the concentration of PGE's in chromite mineral separates due to the well documented occurrence of small (~10μm) inclusions of PGM and PGE sulphides which may overwhelm the true concentration of PGE held in solid solution [9,10,11]. A study

which used LA-ICPMS to examine chromite from the Merensky Reef found no detectable concentrations of PGE's in solid solution with chromite [12]. Another recent LA-ICPMS study, which examined numerous chromites from chomitiites situated in the mantle to the crustal sections of an ophiolite, found no evidence of PGE's save Ru, which was found at 38 to 134 (± 20) ng/g [13].

The association of PGE's and chromite in natural systems prompted an array of experimental study aimed to better understand the role of spinel in PGE fractionation. Pioneer experimental work on spinel partitioning was performed by Capobianco et al. [14] on a CAMS system where the partitioning of Ru, Rh, and Pd was investigated under high fO2's (ΔFMQ 5.0-7.5). Run products contained recrystallized 'rinds' of spinel, as well as euhedral, detached spinels which were analyzed using an electron microprobe [14]. The experimental results reveal Ru and Rh to be compatible in spinel, with D's of ~23 and ~84, respectively, and Pd to be incompatible, with a D value of <0.02[14]. Capobianco et al. [14] note that the relative compatibility of Ru and Rh in natural systems is opposite to their determined experimental values yet emphasize that, in any case, crystal chemical control and so, the relative fractionation of the PGE's by spinel is unmistakable.

Capobianco et al. [15] further investigated spinel partitioning on an iron bearing system where Ru, Rh and Pd partitioning was investigated under fO2's corresponding to ΔFMQ values of 3.5-5.0. Trace element analysis was done by electron microprobe for Pd and by ion microprobe for Ru and Rh [15]. Ru and Rh, with D's of 450->4000 and 110-400, respectively, were found to be compatible in magnetite while Pd, with D's of 0.4-1.2, is found to be incompatible[15]. The addition of Fe to the system is seen to increase the compatibility of Ru and Pd by at least an order of magnitude relative to Capobianco et al.'s earlier results from 1990[14,15]. The order of compatibility in this study is Ru>Rh>>Pd, which agrees with the relative compatibility seen in natural systems [15]. Also noteworthy, are the high partition coefficients determined for Ru which are comparable to sulphide/silicate melt partition coefficients, indicating that spinel may play a significant role in fractionating PGE's in natural systems even after sulfide saturation [15].

More recently, Righter et al. [16] performed partitioning experiments of Ru, Pd and Ir in Cr-bearing spinels at fO2's corresponding to ΔFMQ values of 0.8-6.0. Trace element analysis was performed by SIMS and LA-ICPMS [16]. D values of 100-1143 were reported

for Ru, 41-450 for Rh and 0.14 for Pd [16]. Since the effect of spinel composition on partitioning is unknown, efforts to obtain trends for PGE D's as a function of oxygen fugacity are hampered by the varying composition of the spinels over the fO2 range [16]. Additionally, the Cr and Fe composition of the spinels in different runs at the same oxygen fugacity vary by up to 25wt%; this is an unexpected result and may point to false fO2 assignments [16]. Furthermore, the reported glass concentrations of the PGE's are significantly higher than any previous solubility data has suggested at a given fO2 and appear to increase as fO2 is decreased which is again contradictory to the expected result [16].

Finnigan has done partitioning experiments of all the PGE's into chromite at fO2's corresponding to ΔFMQ 0.0 – 3.8 in an iron bearing system [17]. LA-ICPMS analysis lead to D's of 0.61-215 for Rh, 2.15-28 for Ru, 0.003-0.02 for Pd, <0.69-12.9 for Pt, 9-213 for Os and >70 for Ir [17]. Notably, the D values of Rh and Ru are shown to decrease with decreasing fO2 and it is suggested that this change may be attributed to the decrease in ratio of oxidized/reduced PGE species dissolved in the melt [17].

The effect of oxygen fugacity on the partitioning of the PGE's is potentially great due to the heterovalent nature of these elements. Solubility studies have modeled a change in the oxidation state of the PGE's in silicate melts as a function of fO2, with the crossover in the dominant dissolved PGE species occurring between FMQ-1 to +9, depending on the particular PGE [18,19,20]. From the oxidation states inferred by these solubility studies, predictions can be made about the compatibility of the various species of the PGE's based on the similarity of the charge and size of the dominant dissolved species in the melt to the A and B sites in spinel ($A^{2+}B^{3+}{}_2O_4$). Thus, as a function of fO2, the D-values of the PGE's should reflect this change in oxidation state.

The partitioning of rhenium into numerous silicates as a function of fO2 has been shown to change by several orders of magnitude [21]. This change was solely attributed to Re's 4+ to 6+ change in oxidation state [21]. In this report, results of spinel/melt partitioning experiments performed over a range of fO2's are reported and the results are interpreted in terms of PGE speciation.

Experimental Techniques

One Atmosphere

Experiments were carried out in a gas-mixing vertical tube furnace. Oxygen fugacity was dictated by O_2, air, CO_2, N_2-CO_2 and CO-CO_2 gas mixtures and furnace fO2 was determined using a Y-doped zirconia oxygen probe before initiation and after termination of each experiment. Voltage values from the oxygen probe were converted to log fO2 values by the Nernst equation …

$$EMF_{cell} = EMF^{o}_{cell} - (RT/nF)*(\ln(p_{O2\ in\ reduced}/p_{O2\ in\ oxidized}))$$

… where EMF_{cell} is the potential from the sensor, EMF^{o}_{cell} is the potential at equilibrium i.e. when air is run through the furnace, R is the gas constant, T is temperature in Kelvin, n is the number of electrons involved in the cell reactions, $p_{O2\ in\ reduced}$ is the partial pressure of oxygen in the reduced portion of the cell i.e. the furnace environment and $p_{O2\ in\ oxidized}$ is the partial pressure of oxygen in the oxidized portion of the cell i.e. the reference gas. The reduction half-cell reaction is…

$$4e^- + O_2 \rightarrow 2O^{2-}$$

…and so, n = 4. Assuming EMF^{o}_{cell} is zero, $p_{O2\ in\ oxidized}$ is 0.209 (20.9%O_2 in air), F= 96 485C/mol, R= 8.314J/Kmol and converting EMF to mV and rearranging to find log $p_{O2\ in\ reduced}$ yields…

$$\log p_{O2\ in\ reduced} = \log (0.209*(e\text{^}(-46.2*(EMF/T))))$$

Furnace temperatures were monitored for the duration of the experiment using an alumina sheathed TYPE B Pt-Pt10%Rh thermocouple.

Experiments utilized a starting composition analogous to that of Capobianco et al. [14], which was further saturated in MgO and Al2O3 by the partial dissolution of an alumina-oversaturated synthetic spinel chip (Table 1). The samples consisted of the starting composition, a synthetic spinel chip and in some cases, a metal bead, packed onto a wire-

Table 1
Starting Compositions

SiO2	Al2O3	MgO	CaO
45.87	21.09	19.31	13.73

Composition of starting composition (SC) #5 in wt%. SC#3 was ~2.4wt% undersaturated in spinel while SC#4 and SC#5 were undersaturated by ~1.4wt%. All compositions were doped with 0.5-1.0wt% of NiO and MnO.

loop with PVA and were hung from a silica rod inside the furnace. Wire loop compositions were either pure or alloyed PGE's and were chosen to minimize a change in metal activity during the entirety of the experiment by utilizing immiscible pairs or alloys that do not significantly change in composition in the temperature range of the experiments. A Pt-Rh alloy was used for experiments examining those metals at >FMQ+4.2 while at lower fO2's, a Pd wire with a Au-Rh bead was used in an attempt to parallel a method used by Brenan et al.[22], where Au was found to "preferentially wet" Ir crystals and suppress micronugget formation. An Ir-Au bead was utilized with a Pd wire for all experiments investigating Ir partitioning, except the FMQ+6 experiment which used pure Ir. Due to Pd-Au alloying, the Au-Rh and Au-Ir beads were first pre-saturated in Pd at run temperatures. Experiments examing Ru partitioning used a pure Ru bead with a Pd wire.

Experiments were commenced by slowly lowering the sample into the predetermined hotspot of the furnace after the furnace atmosphere had been allowed to equilibrate at the run fO2. Whence in the hotspot, the samples were allowed to homogenize for durations of 100-136hrs at temperatures between 1390ºC-1400ºC, except for the Au-Rh-Pd experiments whose homogenization temperatures were lowered by ~10ºC to decrease the extent of Rh-Pd alloying. After the homogenization step, the samples were first cooled quickly, to encourage nucleation, and then slowly, to allow for large crystal growth. The fast cooling step persisted for 41ºC at a rate of 60º/hr and the slow cooling step persisted for 20ºC at a rate of 1ºC/hour, except for all runs which are labeled as Cooling Step Seq #1 (listed in Table 2), which underwent fast cooling for 50ºC and slow cooling for 12ºC and all runs after and including SpPdRu40, which experienced slow cooling at a rate of 0.8ºC/hour. After the cooling step, the samples sat at the final temperature for durations of 0.5hrs-6.5hrs before being quenched in a beaker of cold water.

Figure 1. Typical sample + thermocouple assembly.

Table 2
Summary of experiments

Sample	Starting Comp.	PGE source	log fO2	FMQ	Dwell Time (hrs)	Cooling Step Seq
SpPtRh12	3	Pt10%Rh	-2.69	4.21	100	1
SpPtRh16	3	Pt10%Rh	-0.69	6.21	120	1
SpPtRh17	3	Pt10%Rh	0.00	6.90	100	1
SpPtRh18	3	Pt6%Rh	-0.69	6.21	136	2
SpPtRh19	3	Pt6%Rh	0.00	6.90	100	1
SpPdRh23	3	Palladium + pure Rh wire	-0.69	6.21	111.5	2
SpPdRh24	3	Palladium + pure Rh wire	-2.88	4.12	138	2
SpPdRh25	3	Palladium + pure Rh wire	0.00	6.90	134	2
SpPdRu32	4	Pd loop + 11mg Ru bead	-2.56	4.44	113	2
SpIrPd35	4	New Pd loop + Ir beads from 34	-0.69	6.21	67 in CO2, 74 in Air	2
SpPtRh36	4	Pt10%Rh	-3.40	3.60	110	2
SpPtRh39	4	Pt30%Rh	-0.69	6.21	110	2
SpPdRu40	5	Pd wire + pure Ru	-3.10	3.80	100	2
SpPdRhAu48	5	Pd wire + Rh-Au(66%:33%) bead	-3.80	3.10	100	2
SpPdIr54	5	Pd wire + pure Ir	-0.69	6.21	90	2

Each run homogenized at temperatures of 1390ºC-1400ºC and reached final temperatures of 1325ºC-1335ºC. Cooling Step Seq #2 has nine more degrees of slow cooling than #1.

High Pressure

Experiments to measure Os partitioning were performed at 1.3 GPa with samples encapsulated in Pt, and fO_2 fixed using Ru-RuO_2 (~FMQ+6) or Re-ReO_x (~FMQ+1) internal buffers.

Analytical Techniques

Run products were mounted in polycarbonate rounds and polished down to a 1μm polish with alumina powder.

Major Element

Major element analysis was performed by the Cameca SX50 electron microprobe at the University of Toronto. Electron beam conditions during analysis were 15kV and 50nA for glass, spinel and olivine. Standards for glass analysis were Craugitesx1 (Si), grossularsx1 (Al), pyropKsx1 (Mg), diopssx2 (Ca), NiO (Ni) and bustamsx1 (Mn) and standards for spinel were Craugitesx1 (Si, Ca), MgAl2O4sx1 (Mg, Al), pentlasx1 (Ni) and bustamsx1 (Mn). Samples SpPdRu40 to SpPdIr54 used an aluminum oxide standard for Al in the spinel.

Standards for olivine were olivFo100PS90 (Si,Mg), bustamsx1 (Mn), Craugitesx1 (Ca, Al) and pentlasx1 (Ni). Counting times for spinel were 20 sec on Mg and Al, 30 sec on Si, Ca and Mn and 60 sec on Ni. Counting times for the glass were 30 sec on Mg and Al, 40 sec on Si and Mn, and 60 sec on Ni and Ca. Counting times for olivine were 20 sec on Si and Mg, 30 sec on Mn, 40 sec on Al, 60 sec on Ni and 70 sec on Ca. Raw count rates for all analysis were converted to concentrations by the ZAF reduction scheme. Major element compositions (in wt%) of spinel, glass and olivine are provided in Table 3, 4 and 5, respectively.

Table 3
Summary of spinel analyses

Sample name	n	SiO2		MgO		Al2O3		CaO		NiO		MnO		Total
SpPtRh12	18	0.17	0.01	26.78	0.11	69.79	0.18	0.01	0.01	2.29	0.06	0.14	0.01	99.19
SpPtRh16	15	0.15	0.01	26.98	0.19	70.06	0.52	0.01	0.01	2.82	0.06	0.18	0.01	100.20
SpPtRh17	15	0.16	0.02	26.83	0.17	70.16	0.33	0.02	0.01	2.87	0.08	0.20	0.01	100.23
SpPtRh18	17	0.15	0.02	26.98	0.27	70.10	0.62	0.01	0.01	2.72	0.04	0.17	0.01	100.14
SpPtRh19	15	0.15	0.02	26.44	0.13	69.44	0.37	0.02	0.01	2.84	0.11	0.20	0.02	99.08
SpPdRh23	17	0.15	0.02	26.86	0.22	70.13	0.31	0.01	0.01	2.87	0.08	0.18	0.01	100.21
SpPdRh24	14	0.15	0.01	27.00	0.20	70.25	0.49	0.01	0.01	2.50	0.05	0.15	0.01	100.05
SpPdRh25	24	0.15	0.01	26.89	0.18	70.35	0.42	0.01	0.01	2.80	0.08	0.19	0.01	100.40
SpPdRu32	9	0.17	0.01	26.07	0.25	69.41	0.79	0.01	0.01	3.69	0.08	0.26	0.02	99.61
SpPdIr35	6	0.17	0.01	25.80	0.20	70.24	0.46	0.01	0.01	3.41	0.12	0.30	0.01	99.94
SpPtRh36	13	0.18	0.04	26.35	0.23	69.46	0.59	0.01	0.01	3.08	0.10	0.25	0.02	99.34
SpPtRh39	12	0.23	0.02	25.63	0.24	70.35	0.55	0.01	0.01	3.71	0.13	0.30	0.01	100.23
SpPdRu40	16	0.15	0.02	26.39	0.19	69.48	0.48	0.02	0.01	3.71	0.07	0.02	0.01	99.78
SpPdRhAu48	10	0.14	0.01	26.86	0.29	69.66	0.68	0.01	0.01	2.73	0.07	0.19	0.01	99.58
SpPdIr54	14	0.14	0.01	26.33	0.27	69.49	0.57	0.02	0.01	3.59	0.06	0.23	0.01	99.79

Table 4
Summary of glass analyses

	n	SiO2		MgO		Al2O3		CaO		NiO		MnO		Totals
SpPtRh12	16	46.10	0.12	17.16	0.07	21.71	0.07	14.32	0.04	0.29	0.01	0.50	0.02	100.09
SpPtRh16	16	46.42	0.10	17.14	0.05	21.65	0.10	14.36	0.04	0.36	0.01	0.49	0.01	100.41
SpPtRh17	16	46.72	0.13	17.22	0.07	21.68	0.11	14.38	0.04	0.37	0.01	0.47	0.01	100.82
SpPtRh18	16	46.52	0.12	17.07	0.16	21.33	0.14	14.36	0.05	0.33	0.01	0.47	0.01	100.10
SpPtRh19	15	46.19	0.13	16.88	0.07	21.73	0.09	14.43	0.06	0.36	0.02	0.46	0.01	100.04
SpPdRh23	15	46.43	0.09	17.25	0.09	21.58	0.07	14.26	0.05	0.36	0.01	0.48	0.01	100.37
SpPdRh24	15	46.36	0.18	17.19	0.13	21.32	0.14	14.34	0.05	0.31	0.01	0.49	0.02	100.01
SpPdRh25	15	46.92	0.11	17.55	0.09	21.18	0.21	14.29	0.04	0.37	0.03	0.45	0.02	100.76
SpPdRu32	15	46.39	0.09	16.36	0.06	21.76	0.05	15.03	0.04	0.46	0.02	0.66	0.01	100.66
SpPdIr35	13	46.50	0.18	16.82	0.08	21.96	0.10	14.74	0.04	0.45	0.01	0.63	0.02	101.09
SpPtRh36	14	46.36	0.12	16.27	0.07	22.12	0.11	14.89	0.04	0.40	0.02	0.65	0.01	100.69
SpPtRh39	15	46.33	0.22	16.73	0.09	21.79	0.10	14.85	0.04	0.47	0.02	0.64	0.02	100.81
SpPdRu40	14	46.85	0.29	18.12	0.14	20.36	0.14	14.13	0.05	0.57	0.01	0.05	0.01	100.06
SpPdRuAu48	15	46.71	0.17	15.93	0.09	21.15	0.17	15.25	0.04	0.33	0.02	0.56	0.02	99.93
SpPdIr54	15	46.70	0.16	16.49	0.09	21.82	0.12	14.52	0.05	0.52	0.02	0.53	0.02	100.58

Table 5
Summary of olivine analyses

	n	SiO2		MgO		Al2O3		CaO		NiO		MnO		Totals
SpPtRh17	11	42.24	0.14	55.56	0.12	0.20	0.05	0.30	0.01	2.57	0.05	0.33	0.01	101.19
SpPtRh18	15	42.12	0.11	55.47	0.11	0.24	0.09	0.30	0.01	2.36	0.08	0.35	0.02	100.84
SpPtRh19	14	41.87	0.23	55.03	0.25	0.30	0.10	0.30	0.01	2.54	0.08	0.32	0.02	100.37
SpPdRh23	14	42.05	0.20	55.27	0.40	0.30	0.10	0.30	0.01	2.51	0.07	0.35	0.02	100.77
SpPdRu32	15	41.92	0.18	54.22	0.23	0.19	0.05	0.31	0.01	3.49	0.11	0.48	0.02	100.62
SpPdIr35	17	42.22	0.19	54.29	0.77	0.24	0.08	0.35	0.10	3.21	0.10	0.45	0.02	100.76
SpPtRh36	15	41.96	0.31	54.46	0.43	0.21	0.08	0.32	0.01	2.85	0.06	0.48	0.02	100.28
SpPtRh39	13	41.86	0.26	54.22	0.36	0.20	0.05	0.31	0.01	3.37	0.11	0.45	0.01	100.40

Trace Element

Trace element analysis was performed by laser ablation inductively coupled plasma mass spectrometry(LA-ICP-MS) at the University of Toronto for samples 12-39 and at McGill University for samples 39-54. Spot sizes were varied according to new growth spinel crystal size and usually ranged from 60-100µm. Glass sizes were 120µm. Typical analysis consisted of 20seconds of background acquisition, 60seconds of sample acquisition and then about two minutes of flushing with He. Standards used were NIST 610 and JB-sulphide. Samples were analyzed for Ru101, Pt194, Rh102, Pd105 and Ir192. Trace element concentrations are listed in Table 6.

Table 6
Summary of trace element concentrations(ppm) and partition coefficients

Element	Sample	FMQ	Glass		Spinel		D(spinel)		Olivine		D(olivine)	
Rh	SpPtRh12	4.21	0.36	0.02	47.81	2.22	133.3	8.9	-	-	-	-
	SpPtRh16	6.21	8.3	0.8	976	50.3	118	12.8	-	-	-	-
	SpPtRh17	6.90	20.7	0.2	2784.8	358.7	134.4	17.4	147.9a	-	7.14	0.07
	SpPtRh18	6.21	5.4	0.1	879.2	99.6	162.5	18.7	24.8a	-	4.6	0.1
	SpPtRh19	6.90	12.8	0.4	1826.5a	-	143.1	4.1	70.6a	-	5.53	0.16
	SpPtRh36	3.60	0.251*	-	32.4	0.8	129.1	3.1	0.59	0.02	2.38	0.09
	SpPtRh39	6.21	16.4	1.15	2941.5	156.9	179.2	15.8	-	-	-	-
	SpPdRhAu48	3.10	0.02*	-	3.6	0.9	182.1	-	-	-	-	-
			0.025b	-	3.6	0.9	143.2	-	-	-	-	-
Pt	SpPtRh12	4.21	0.55	0.03	0.078*	-	0.14	0.01	-	-	-	-
	SpPtRh16	6.21	8.7	0.2	9.9	1.3	1.14	0.15	-	-	-	-
	SpPtRh17	6.90	15.63	0.13	38.1	1.5	2.4	0.1	0.48a	-	0.031	0.03
	SpPtRh18	6.21	8.7	0.1	10	0.5	1.15	0.06	0.32a	-	0.037	0.001
	SpPtRh19	6.90	15.3	0.6	42.1a	-	2.75	0.11	-	-	-	-
Ru	SpPdRu32	4.44	3.8	0.5	156.9	10.8	41.8	6	5.35	1.1	1.43	0.34
	SpPdRu40	3.80	0.62	0.11	34.2	3.4	54.8	11.2	-	-	-	-
Ir	SpPdIr54	6.21	0.11	0.08	9.5	2.6	90.1	75.3	-	-	-	-
Pd	SpPdRh23	6.21	308.8	15.9	1.51	0.04	0.0049	0.0003	8.93	0.21	0.029	0.002
	SpPdRh25	6.90	2536.3	235.5	17.5	0.9	0.0069	0.0007	-	-	-	-
	SpPdRu32	4.44	83.9	3.5	0.39	0.05	0.0023	0.0003	1.11	0.06	0.013	0.001
	SpPdIr35	6.21	229.3	18.1	3.33a	-	0.015	0.001	7.14	0.96	0.031	0.005
	SpPdIr54	6.21	361	3	2.08	0.14	0.0057	0.0004	-	-	-	-
Os	-	6.01	-	-	-	-	2	-	-	-	-	

* lowest value
a based on one analysis
b avg of non-less than values

LA-ICPMS spectra from selected experiments are shown in Figure 2.

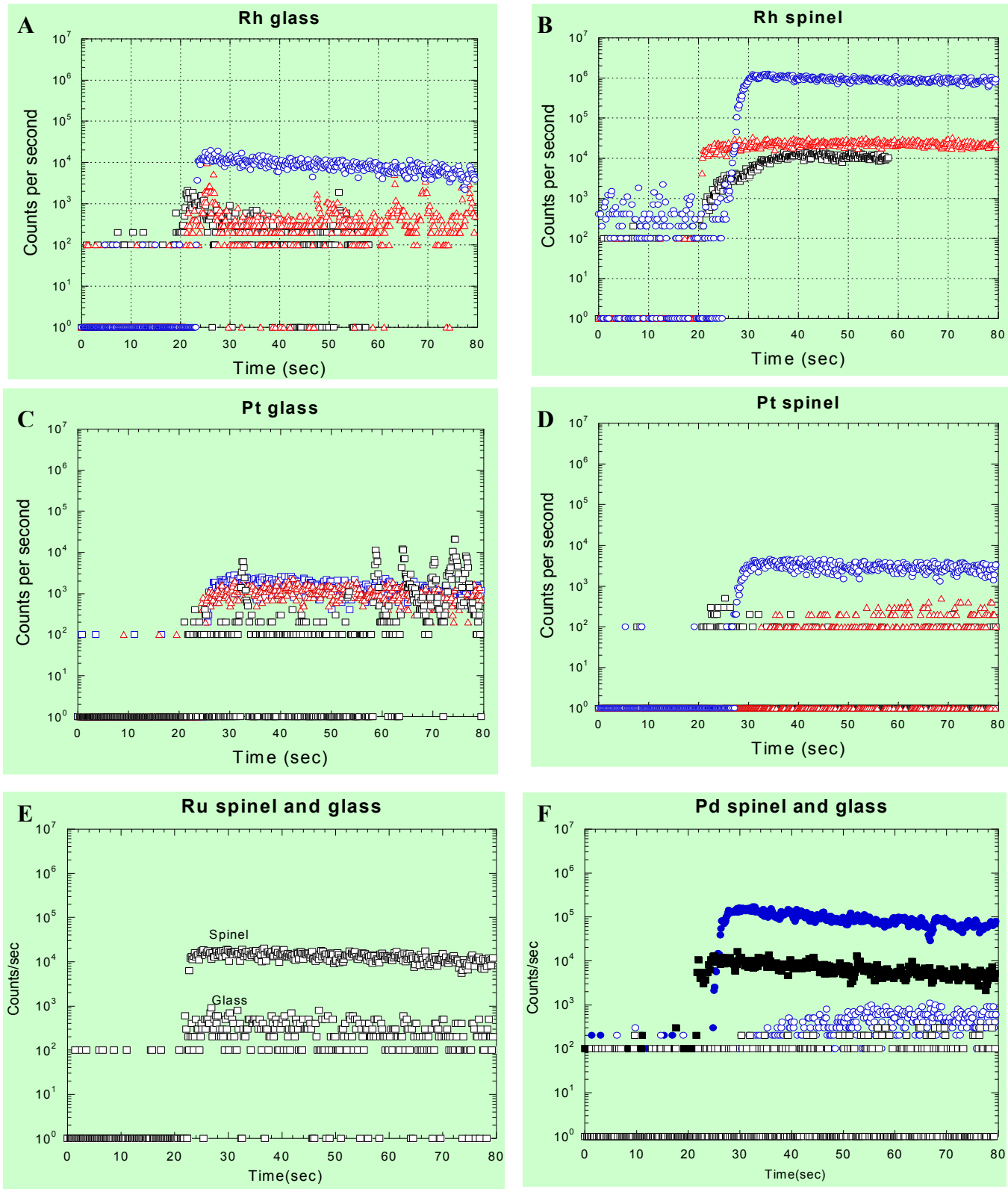

Figure 2. Time resolved spectra. Red=FMQ+6.9, Blue= FMQ+6.21, Black= FMQ+4.21. In F, solid shapes are glass and empty shapes are spinel spectra.

Results and Discussion

Run Product Observations

A typical run-product of the one atmosphere experiments is shown in Figure 3A.

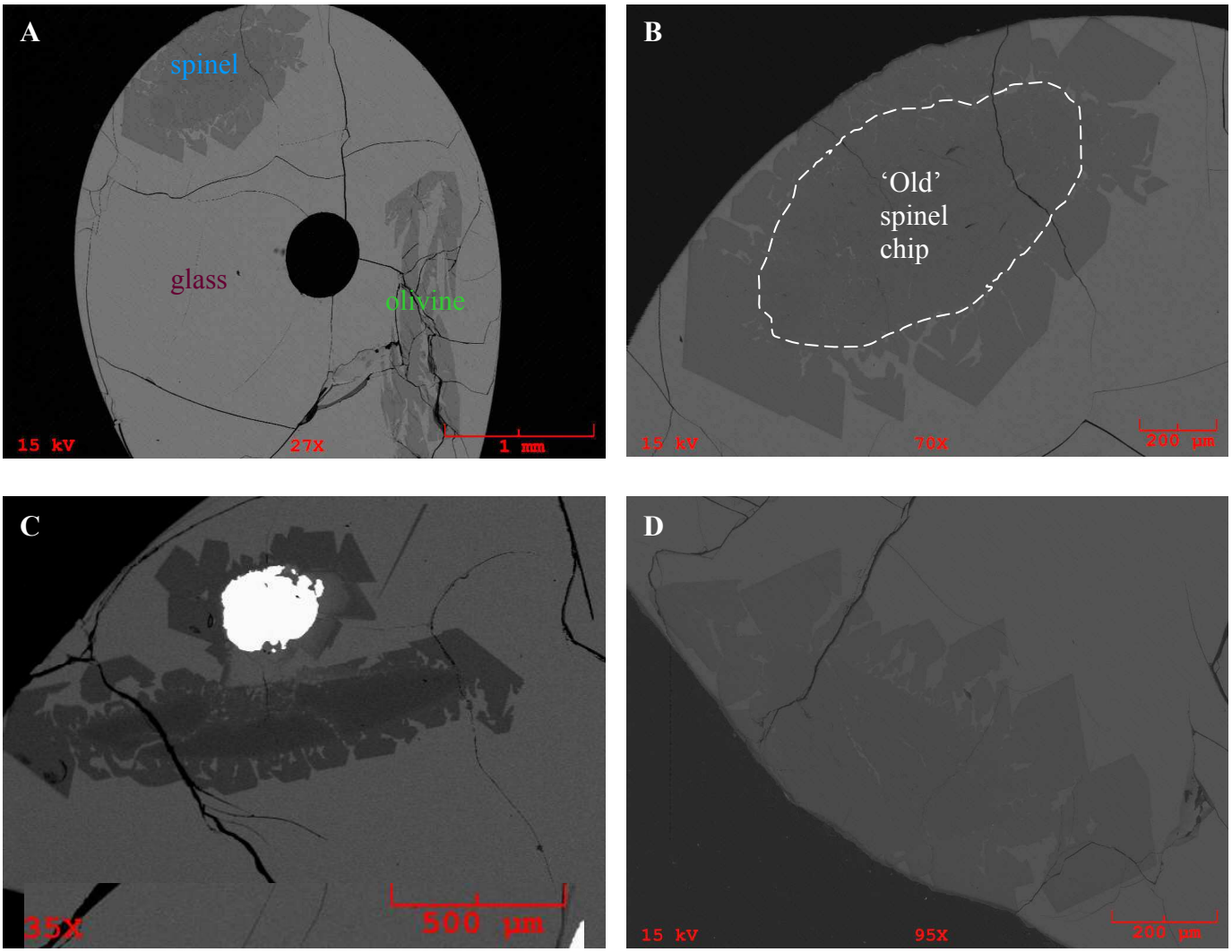

Figure 3. SEM images A- SpPtRh18: Showing a typical polished sample with spinel, olivine and glass phases. Black circle is a hole in-filled with epoxy. B- SpPtRh18: Close-up of spinel showing the outline of the 'old' spinel chip used as the site of nucleation, which usually retained some corundum in it's core, and the new growth surrounding it. C- SpPdRh25: Showing nucleation on pure Rh wire and largest crystals on 'short sides of rectangle' (see text). D- SpPtRh12: Showing largest crystals on 'short sides of rectangle' (see text).

Spinel

New spinel growth generally occurred as blue, euhedral crystals which were heterogeneously nucleated on a partially dissolved 'old' spinel chip. The largest and most euhedral growth tended to occur on the short sides of the old spinel chip if the old spinel chip is viewed as a

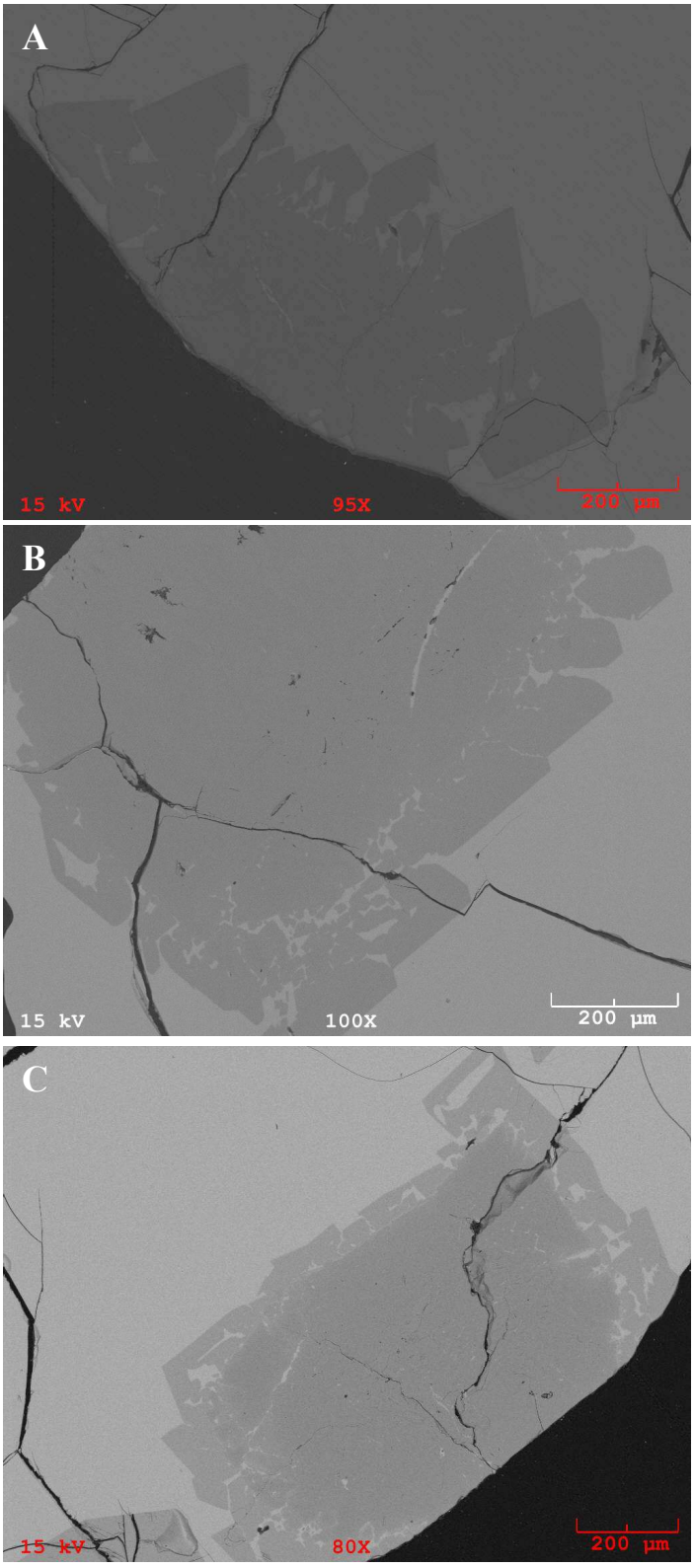

Figure 4. SEM images showing the changing morphology of new growth spinel with increasing Rh content. A- Pt10Rh:FMQ+4.21 B- 66%Rh with 33%Au:FMQ+3.10 C- Pure Rh:FMQ+6.21

rough rectangle, as is most evidently seen in Figure 3C and 3D. This may have been due to the greater volume of melt available, for the crystal to 'stretch out' into, that was uninhibited by other growing crystals, which were depleting the melt of Mg and Al. The two major factors which effected the overall size and morphology of new spinel growth within each experiment were 1) size of the 'old' spinel chip and so, the surface area available for heterogeneous nucleation and 2) the length of the slow cooling step, with the first factor being more influential than the second. The first factor is well demonstrated by preliminary experiments where a spinel crucible packed with melt was run with the same time-temperature history as the runs in Figure 3 yet produced ~20-50µm new growth. The second factor is demonstrated by Figure D, which shows a smaller chip with a shorter slow cooling step, and Figure B, which shows a larger chip with a longer slow cooling step. This factor may be attributed to the extra 9 degrees of slow cooling during the longer slow cooling step which allows for a greater

amount of time committed to euhedral growth.

Homogeneously nucleated, blue, spinel crystals were found only in experiments where the source of PGE was pure Ir or Rh. These spinels ranged in size from 50- ~120μm in diameter.

Experiments with varying activities of Rh seemed to control the morphology of the spinels, where more cube shaped spinels seemed to grow with increasing a_{Rh}, as is illustrated in Figure 4. The greater concentration of Rh in the spinels seemed to inhibit large crystal growth although this may have been caused by the additional growth occurring in other parts of the sample by homogeneously nucleated spinels. Finally, the changing morphology of the spinel as a function of Rh concentration may further illustrate that Rh is actually being incorporated into the spinel lattice.

Olivine

New olivine growth generally occurred as green, homogeneously nucleated, skeletal crystals with the exception of SpPdIrAu33 where a euhedral olivine had grown and SpPdRu32, where no olivine could be found. Olivines generally showed no preference, in terms of site of nucleation, but often appeared to reside at the top of the sample where the wire loop was twisted.

Metal Alloys

Metal alloys were found in some experiments in which fO2 was =<FMQ+4.2, although one experiment at FMQ+6.21 also produced alloys. Alloys frequently occurred in experiments where a change in metal activity within the duration of the experiment was evident (e.g. Rh source cut off by crystallizing spinel and measured [Rh] varied within sample or complete Ir vapourization) yet alloys also occurred in samples where metal activity was assumed constant and were present in two experiments where partition coefficients were calculated. Generally, alloys were <10μm in diameter and seemed to reside on the boundaries of the 'old' spinel chip, except for one alloy which was caught in a growing crystal. Images of alloys are shown in Figure 5.

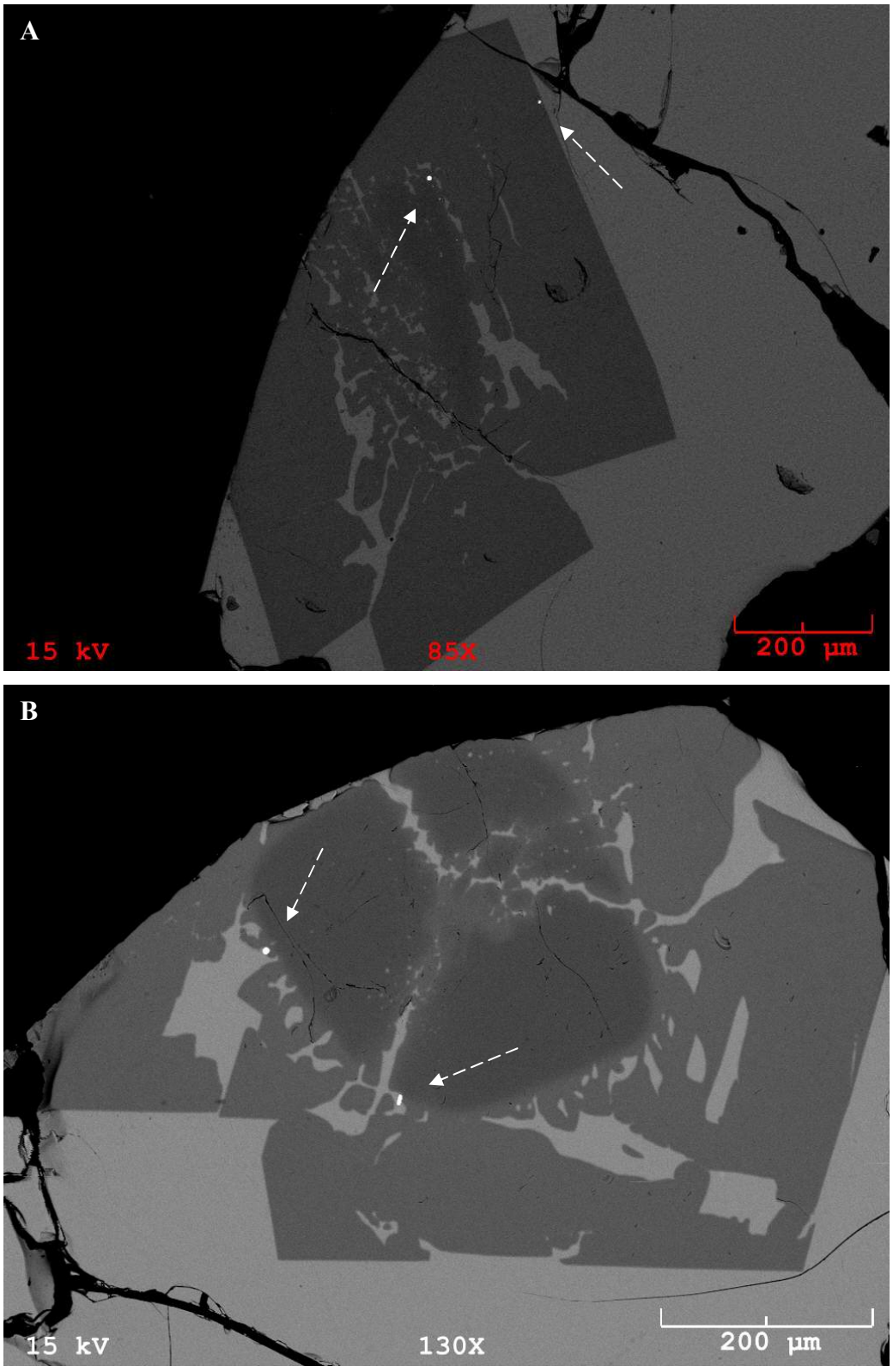

Figure 5: Metal alloys. A- SpPdRh24:FMQ+4.21- Alloy evident on the edge of the 'old' spinel chip and caught in the new growth. B- SpPdIrAu33:FMQ+4.21- One of the alloys appears to be an amalgamation of two alloy spheres. Ir vapourized during this experiment.

Major Element Behaviour

Analysis from the core to the rim of new growth crystals, as well as random points shows major element homogeneity of spinel. Glass analyses were conducted at random points throughout the entirety of the exposed glass area and also show homogeneity.

Trace Element Behaviour

LA-ICPMS analysis of spinel and glass show trace element homogeneity in time resolved spectra, except in lower fO2 experiments where micronuggets were encountered. Seen in Figure 2.

Available Sites for PGE in Spinel

The general formula for the spinel mineral group is…

$$(A^{2+}_{1-x}B^{3+}_{x})[A^{2+}_{x}B^{3+}_{2-x}]O_4$$

…where round brackets represent tetrahedral sites, square brackets represent octahedral sites and x is the inversion parameter [23]. The inversion parameter is a function of composition, temperature and pressure and a value for Mg,Al-spinel at ~1400ºC and 1atm of 0.3 is adopted here yielding a formula of [24, 25, 26]…

$$(A^{2+}_{0.7}B^{3+}_{0.3})[A^{2+}_{0.3}B^{3+}_{1.7}]O_4$$

Therefore, 2+ and 3+ octahedral sites with radii of 0.72 and 0.535 angstroms, respectively, are available [27]. The small fraction of the 2+ octahedral sites vs. 3+ octahedral sites should not perturb 2+ partitioning assuming that the experiment duration will suffice the rate at which the PGE enters the site and that there is no competition by any 2+ species dissolved in the melt for the 2+ site [28].

The addition of Cr to Mg,Al-spinel pushes the inversion parameter towards zero [29]. In Fe-Cr spinels, when the Cr^{3+} occupation of the octahedral site is >= ~63% stoichiometrically, then x=~0 [30].

Oxidation state of PGE dissolved in silicate melts

The oxidation state of a metal dissolved in a silicate melt may be modeled based on the dependence of metal solubility on oxygen fugacity, as seen by the equation [19]…

$$M^{x+} + (x/4)O_2 \leftrightarrow MO_{x/2\ (\text{in melt})}$$

The equilibrium expression for this reaction is…

$$K = a_{MOx/2\ (\text{in melt})} / [a_{Mx+} \cdot fO_2^{x/4}]$$

Assuming the activity of a pure metal is 1…

$$K = [\gamma_{MO} \cdot X_{MOx/2\ (\text{in melt})}] / fO_2^{(x/4)}$$

where γ_{MO} is the activity coefficient and $X_{MOx/2\ (\text{in melt})}$ is the mole fraction of the metal oxide in the melt [19]. At low concentrations, dissolved metal oxide behaviour approaches ideal behaviour and so, the activity coefficient becomes 1…

$$\log [MO_{x/2}] = x/4 \log fO_2 + C$$

where $[MO_{x/2}]$ is the concentration of the metal oxide and C is a constant comprised of the fO2 independent log K value plus the conversion factor for mole fraction to concentration [19].

	Reduced species (A)	Oxidized Species (A)
Rh (2+, 3+)	0.72	0.665
Ru (2+, 3+)	0.75	0.68
Os (2+, 3+)	-----	0.68
Ir (2+, 3+)	0.74	0.68
Pt (2+, 4+)	0.80 (0.6)	0.625
Pd (1+, 2+)	0.59	0.86 (0.64)

Table 7. Sizes of PGE species in octahedral coordination. Round brackets beside sizes of Pt and Pd show square-planar size [27].

Solubility studies have utilized the above relationship to model the oxidation state of the PGE's dissolved in silicate melts by linear regression of the slope on a log $[MO_{x/2}]$ vs. log fO_2 plot. From these studies, Pd is thought to be dissolved in silicate melts as a mixture of Pd2+

and Pd1+ [19]. Pt and Rh were both found to be prominently dissolved in the melt as Pt2+ and Rh2+, yet at the highest fO2's (those dictated by pure air and oxygen), a better fit to the experimental data can be attained by the incorporation of some Pt4+ and Rh3+ [18]. Ru is thought to exist in the 3+ oxidation state at high fO2s and 2+ at low fO2's [20].

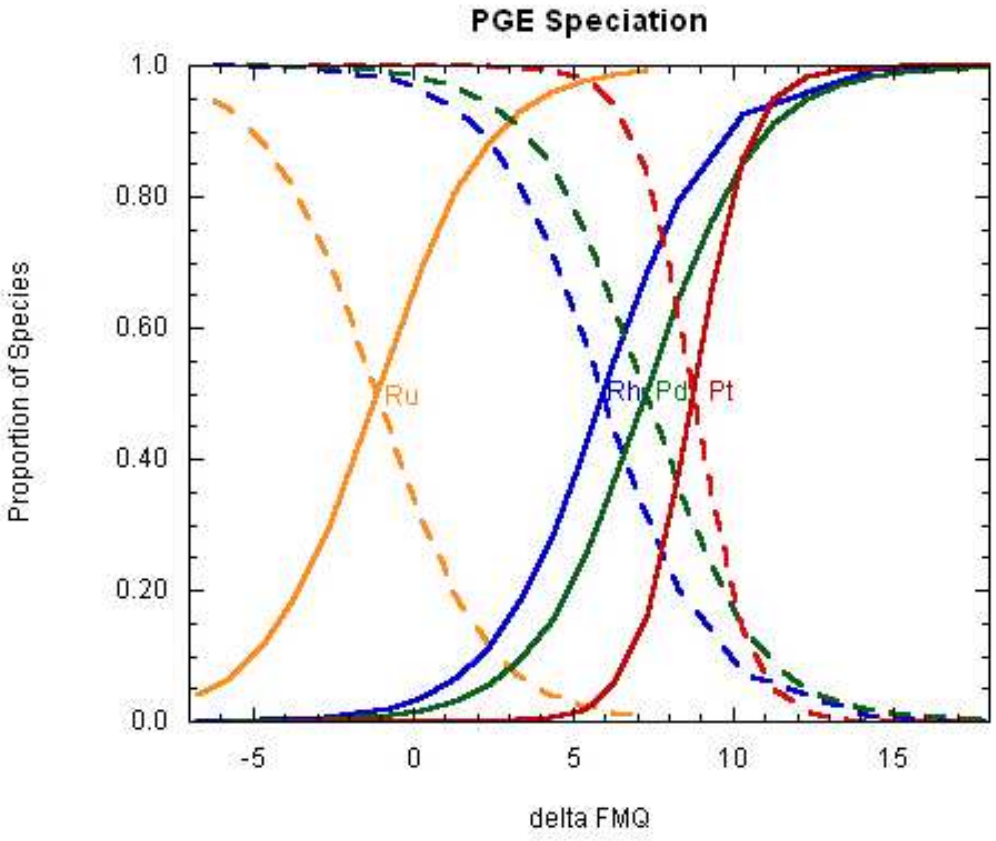

Figure 6. Ru, Rh, Pd and Pt speciation vs. delta FMQ showing the oxidized species as a solid line and reduced species as a dashed line. Pt occurs as 2+ and 4+, Pd as 1+ and 2+, Rh and Ru as 2+ and 3+ [18,19,20].

Partition Coefficients

Spinel

A summary of partition coefficients are shown in Figure 7. The order of compatibility is $D^{Rh} > D^{Ir} > D^{Ru} >> D^{Pt} > D^{Pd}$.

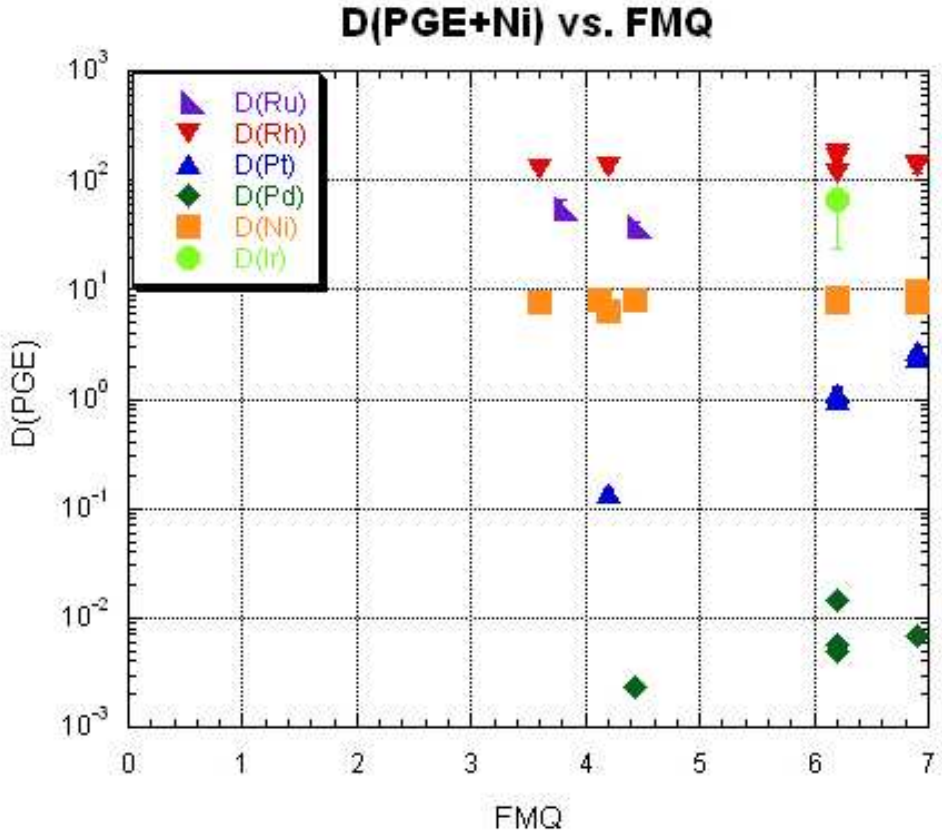

Figure 7. Summary of spinel partition coefficients from the 1atm experiments.

Based on comparisons of the size of Rh^{2+} and Rh^{3+} with the 2+ and 3+ octahedral sites in spinel, Rh is predicted to be compatible and D^{Rh} should increase as fO2 is decreased due to the greater agreement of Rh^{2+} with the 2+ site. Rh partition coefficients were determined from the highest fO2 (FMQ+6.9) down to FMQ+3.10, where glass analyses became exceedingly heterogeneous, and within the entire fO2 range studied, D^{Rh} remains constant with an average value of 140. The lowest fO2 experiment plotted in Figure 7 for Rh (SpPtRh36 at FMQ3.6) contained glass concentrations of 0.251-1.05ppm and the plotted D was calculated using the lowest glass concentration. SpPdRhAu48 at FMQ+3.10, which is not plotted in Figure 7, contained glass concentrations of <0.02–0.03ppm and returns

D-values of >180, if the lowest glass concentration is used, and ~140, if an average of the absolute glass values are used.

The D^{Rh} values measured here agree well with other experimental studies, as seen in Figure 8. D^{Rh} of Capobianco et al. (1990)[14] are slightly lower than those measured here. These differences may be attributed to differences in experimental temperatures and trace element analyses, which were performed by electron microprobe in Capobianco et al. (1990)[14] and, in the experiment in air, show a large range of Rh concentrations with the

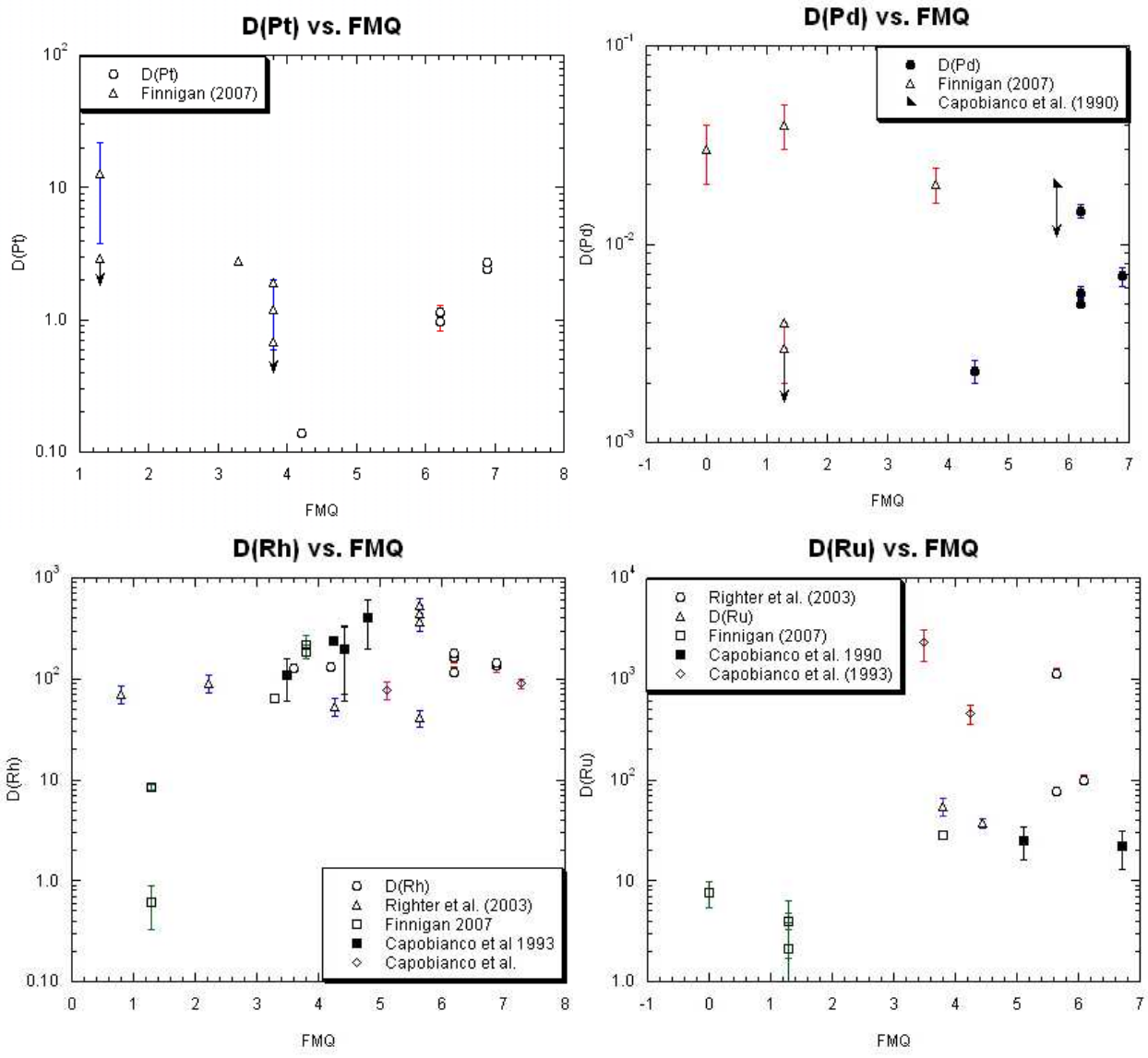

Figure 8. Comparison of D's for Pt, Pd, Rh and Ru found in other experimental studies.

lower end approaching the detection limit of the probe. The differences in D^{Rh} of the other studies can be largely attributed to differences in melt and spinel composition, since their Fe±Cr bearing melt compositions predominantly grew magnetite (Capobianco et al. (1994)[15]) and Cr-bearing spinels (Righter et al. [16]/Finnigan [17]). Despite these differences, the D^{Rh}'s in the FMQ+3.5-FMQ+4.0 range are in particular agreement.

Like Rh, Ir is predicted to be compatible in spinel and due to greater likeness of the size of Ir^{2+} with the 2+(VI) site, D^{Ir} is expected to increase as fO2 is decreased. The D^{Ir} of 90.1 at FMQ+6.21 confirms the compatibility of Ir in spinel yet determination of a trend in D^{Ir} as a function of fO2 was hampered by Ir's high vapourization rate at higher fO2's and by heterogeneous glass analyses at lower fO2's.

The D^{Ir} value reported here agrees with Finnigan's [17] reported D^{Ir} of >70 at FMQ+3.8 yet is lower than Righter et al's [16] D^{Ir} range of 230-22000 at FMQ+4.2.

D^{Ru} is also expected to be greater than one and increase with decreasing fO2. Ru experiments were again limited by a high rate of vapourization at high fO2's and by low glass concentrations at low fO2's yet in the studied fO2 range of FMQ+3.8-FMQ+4.4, D^{Ru} shows a slight increase from 42 to 55 as fO2 decreases.

D^{Ru} measured here are slightly higher than those reported by Capobianco et. al (1990) [14] and by Finnigan [17] at the same fO2. These differences may be attributed to the same experimental and analytical aspects as stated above for Rh.

Pt should behave incompatibly at high fO2's, where there is thought to be a small contribution from Pt^{4+}, and compatibly at lower fO2's, where the size of Pt^{2+} is just slightly larger than that of the 2+(VI) site, yet measured D^{Pt} over the fO2 range of FMQ+6.9 – FMQ+4.12 indicates compatibility at high fO2's and a decrease in D^{Pt} to incompatible values at low fO2's. The clean spectra and precise D^{Pt} values of the high fO2 experiments indicate that they are reliable whereas while the FMQ+4.12 experiment yields precise Pt glass concentrations after filtering out of micronuggets, the spinels yield a range of concentrations from <0.176-0.251ppm. From these values, the greatest agreement between Pt^{194} and Pt^{195} isotope values occurs with the lowest of the absolute Pt^{194} values of 0.78ppm (Pt^{195}=0.81ppm) which was well above the detection limit of 0.065ppm. This value was used to calculate the FMQ+4.12 D^{Pt} value of 0.14. The decrease in D^{Pt} as fO2 decreases may be due to Pt^{2+}'s preference for square-planar co-ordination, as recognized in olivine data, and

the compatibility of Pt in the high fO2 experiments may be due to a coupled substitution with Pt^{4+} [31].

Comparison of the low fO2 D^{Pt} value with Finnigans [17] values at FMQ+3.8 reveal higher D^{Pt} for the chromites.

Pd^{2+} is expected to be slightly compatible with the 2+(VI) site while Pd^{1+} should behave incompatibly. However, experiments at the highest fO2 (FMQ+6.9) indicate strong incompatibility and as expected, D^{Pd} decreases as fO2 is decreased. Some scatter is evident in the FMQ+6.21 as D^{Pd} values vary from ~0.0054, for samples SpPdRh23 and SpPdIr54, to 0.015 for sample SpPdIr35. The D^{Pd} of sample SpPdIr35 can be explained by anomalously low glass concentrations and possibly anomalously high spinel concentrations. The glass concentration of SpPdIr35 (229±18ppm) is much lower than that of SpPdIr54 (360±3ppm) and is also lower than that of SpPdRh23 (308±16ppm), even though this experiment is expected to have lower concentrations of Pd due to the decrease in a_{Pd} caused by Pd-Rh alloying. The anomalously low concentration in SpPdIr35 may have been caused by it's time-fO2 history, which differed from the other FMQ+6.21 experiments. SpPdIr35 homogenized for 67hrs at FMQ+4.21 first and then for 74hrs at FMQ+6.21, while the other experiments homogenized at FMQ+6.21 for 90-111.5hrs. Consequently, the low glass concentration of SpPdIr35 may have been caused by the sluggish rate of increase in the concentration of Pd in the glass which inhibited a new equilibrium (at FMQ+6.21) to establish before cooling and quenching. Logically, however, this would result in a lower than normal D^{Pd} because the spinels would have grown during a time when the concentration of Pd in the melt was lower than what it was at quenching. This raises concern about the higher than normal concentrations of Pd found in the spinel of SpPdIr35(3.3ppm) versus those of SpPdIr54(1.8ppm) and SpPdRh23(1.5ppm). These high concentrations may have been due to the abnormal way in which the spinel and olivine had 'intergrown' in this sample, which produced very unclear boundaries between the two phases and so, the single spinel analysis completed in this run by LA-ICPMS may have clipped a nearby olivine(7ppm), or less likely, glass(229ppm). This confusion between the spinel and olivine phases in this sample was demonstrated in the microprobe analysis as well, where 6 points which were labeled as spinel points actually analyzed olivine.

D^{Pd} measured here agree with Capobianco et al.(1990) [14] where a maximum value of 0.02 at FMQ+5.8 was reported. D^{Pd} values of Finnigan [17] are generally higher than those measured here.

Olivine

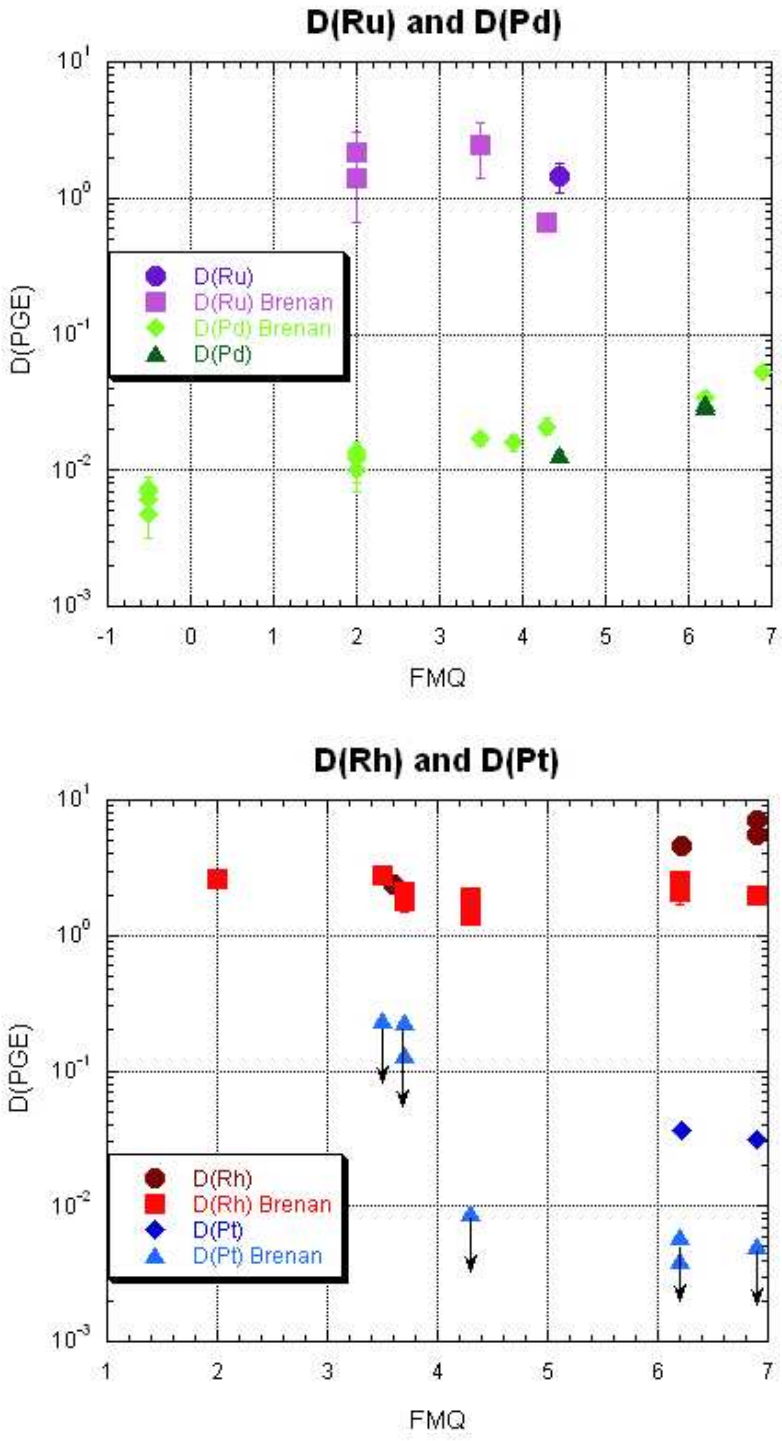

Figure 9: Olivine partition coefficients. Values of D's are listed in Table 6.

Modeling D as a function of oxygen fugacity

In order to overcome the effect of micronuggets and the low concentrations of the PGE's at low fO2, a model in which the oxidation state change is assumed the dictating factor controlling PGE partitioning as a function of fO2 may be used. The bulk partition coefficient, $D_{bulk} = [\Sigma PGE^{x+}O_{x/2}]_{in\ crystal}/[\Sigma PGE^{x+}O_{x/2}]_{in\ melt,}$ combined with the individual oxidized and reduced species partition coefficients, $D_{oxi} = [PGE^{y+}O_{y/2}]_{in\ crystal}/[PGE^{y+}O_{y/2}]_{in\ melt}$ and $D_{red} = [PGE^{z+}O_{z/2}]_{in\ crystal}/[PGE^{z+}O_{z/2}]_{in\ melt}$, yields [31]…

$$D_{bulk} = \frac{D_{red}*[PGE^{z+}O_{z/2}]_{in\ melt} + D_{oxi}*[PGE^{y+}O_{y/2}]_{in\ melt}}{[PGE^{z+}O_{z/2}]_{in\ melt} + [PGE^{y+}O_{y/2}]_{in\ melt}}$$

Plugging in melt concentrations from solubility data yields a sigmoidal curve versus oxygen fugacity.

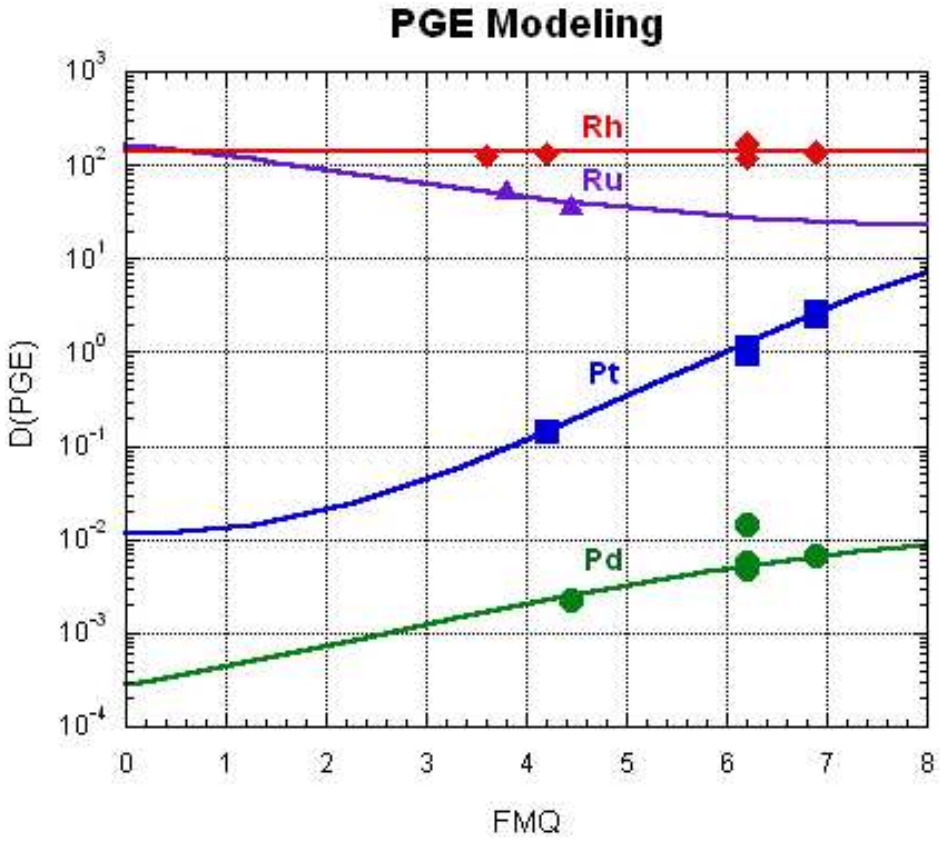

Figure 10. Model applied to data. Reduced and oxidized species D's are as follows **Rh:140-140, Ru:320-20, Pt: 0.01-25, Pd: 0.00005-0.015**

A good fit is obtained for Ru, Pt and Pd suggesting that the oxidation state change is the major factor governing the partitioning of these elements as a function of oxygen fugacity. The only way to model the Rh data is to assume a constant Rh^{2+} and Rh^{3+} partition coefficient but this is not a sound assumption as the 2+ cation agrees with the 2+(VI) site in spinel to a greater extent than the 3+ cation with the 3+(VI) site [27]. Possible explanations for Rh's anomalous behaviour is the effect of melt composition on shifting the oxidation state change to different fO2's or the complete absence of an oxidation state change for Rh.

Conclusions

This report has demonstrated that Mg,Al-spinel accepts Ru, Rh, Ir and Os to a greater extent than Pt and Pd and so, may fractionate the IPGE's from the PPGE's (save Rh). It was shown that the partition coefficients of Ru increase slightly and those of Pt and Pd decrease as fO2 is decreased and that these changes may be attributed to changes in oxidation state of the PGE's dissolved in the silicate melt. According to modeling of the partition coefficients, spinel partition coefficients at fO2's relevant to petrogenesis are expected to be in the order of $D^{Ru} > D^{Rh} >> D^{Pt} > D^{Pd}$.

References

[1] Pearson et al., Re-Os isotope systematics and platinum group element fractionation during mantle melt extraction: a study of massif and xenolith peridotite suites, Chemical Geology 208 (2004) 29-59

[2] Sattari et al., Experimental Constraints on the Sulfide- and Chromite-Silicate Melt Partitioning Behaviour of Rhenium and Platinum-Group Elements, Economic Geology 97 (2002) 385-398

[3] Fleet et al., Laboratory partitioning of platinum-group elements (PGE) and gold with application to magmatic sulfide-PGE deposits, Lithos 47 (1999) 127-142

[4] Laguet et al., Residual platinum-group minerals from highly depleted harzburgites of the Lherz massif (France) and their role in HSE fractionation of the mantle, Geochim. Cosmochim. Acta 71 (2007) 3082-3097

[5] Roger H. Mitchell, Abundance and distribution of gold, palladium and iridium in some spinel and garnet lherzolites: implications for the nature and origin of precious metal-rich intergranular components in the upper mantle, Geochim. Cosmochim. Acta 45 (1981) 2425-2442

[6] Barnes et al., The behaviour of platinum-group elements during partial melting, crystal fractionation, and sulphide segregation: An example from the Cape Smith Fold Belt, northern Quebec, Geochim. Cosmochim. Acta 57 (1993) 79-87

[7] Puchtel et al., Platinum group element fractionation in a komatiitic basalt lava lake, Geochim. Cosmochim. Acta 65 (2001) 2979-2993

[8] Zhou et al., Controls of platinum-group elemental distributions of podiform chromitites: A case study of high-Cr and high-Al chromitites from Chinese orogenic belts, Geochim. Cosmochim. Acta 62 (1998) 677-688

[9] Malitch et al., Laurite and Ruarsite from podiform chromitites at Krasubath and Hockgrossen, Austria: New insights from osmium isotopes, Canadian Mineralogist 41 (2003) 331-352

[10] Torres-Ruiz et al., Platinum-group minerals in chromitites from the Ojen lherzolite massif (Serrania de Ronda, Betic Cordillera, Southern Spain), Mineralogy and Petrology 56 (1996) 25-50

[11] Gutierrez-Narbona et al., New data on base metal mineralogy and platinum-group minerals in the Ojen chromities (Serrania de Ronda, Betic Cordillera, southern Spain), N.Jb.Miner.Abh. 179 (2003) 143-173

[12] Ballhaus et al., Noble metal enrichment processes in the Merensky Reef, Bushveld Complex, Journal of Petrology 41 (2000) 545-561

[13] Philippe Page, SJ Barnes, Richard Cox, Laser ablation study of trace elements in chromite: Thetford Mines ophiolite chromitite ores, Geochim. Cosmochim. Acta, Vol. 71, Issue 15, Supplement 1 (2007) A748

[14] Capobianco et al., Partitioning of ruthenium, rhodium, and palladium between spinel and silicate melt and implications for platinum-group element fractionation trends, Geochim. Cosmochim. Acta 54 (1990) 869-874

[15] Capobianco et al., Experiments on crystal/liquid partitioning of Ru, Rh and Pd for magnetite and hematite solid solutions crystallized from silicate melt, Chemical Geology 113 (1993) 23-43

[16] Righter et al., Partitioning of Ru, Rh, Pd, Re, Ir, and Au between Cr-bearing spinel, olivine, pyroxene and silicate melts, Geochim. Cosmochim. Acta 68 (2004) 867-880

[17] Craig Finnigan, An experimental study investigating the role of chromite on affecting the behaviour of the platinum group elements in igneous systems, Ph.D. Thesis (2006)

[18] Ertel et al., Solubilities of Pt and Rh in a haplobasaltic silicate melt at 1300ºC, Geochim. Cosmochim. Acta 63 (1999) 2439-2449

[19] Borisov et al., Solubility of palladium in silicate melts: Implications for core formation in the Earth, Geochim. Cosmochim. Acta 58 (1994) 705-716

[20] Borisov et al., Ru solubility in silicate melts – Experimental results in oxidizing region, Lunar and planetary science XXIX (1998) Abstract

[21] Mallmann et al., The effect of oxygen fugacity on the partitioning of Re between crystals and silicate melt during mantle melting, Geochim. Cosmochim. Acta 71 (2007) 2837-2857

[22] Brenan et al., An experimental study of the solubility and partitioning of iridium, osmium and gold between olivine and silicate melt, Earth and Planetary Science Letters 237 (2005) 855-872

[23] Rozenberg et al. (2007) Structural characterization of temperature- and Pressure-induced inverse→←normal spinel transformation in magnetite, Physical Review B, 75, 020102-1

[24] An Introduction to The Rock Forming Minerals, Deer Howie Zussman, 2nd Edition, Pearson Education Limited (1992)

[25] Andreozzi et al. (2000) Cation ordering and structural variations with temperature in MgAl2O4 spinel: An X-ray single-crystal study, American Mineralogist, Vol 85, pp. 1164-1171

[26] Wittlinger et al. (1998) Pressure-Induced Order-Disorder Phase Transition of Spinel Single Crystal, Acta Cryst., B54, pp. 714-721

[27] R.D. Shannon, Revised Effective Ionic Radii and Systematic Studies of Interatomic Distances in Halides and Chalcogenides, Acta Crystallographica. A32 (1976) 751-767

[28] Prof. Henderson, pers. comm.

[29] Lavina et al., Cation distribution and cooling rates of Cr-substituted Mg-Al spinel from the Olkhon metamorphic complex, Russia, Eur. J. Mineral. 15 (2003) 435-441

[30] Kurepin, A thermodynamic model of Fe-Cr spinels, Contrib Mineral Petrol 149 (2005) 591-599

[31] Brenan JM, Frontiers Cambridge PP presentation